Article

Use of Biodiesel Press Cake Waste to Prepare Fe/Carbon Reactive Composites for Environmental Applications: Removal of Hazardous Cr^{VI} Contaminants

Elizângela A. Santos,[a] Paulo F. R. Ortega,[a] Rodrigo L. Lavall,[a] Sérgio C. Reis,[b]
José D. Ardisson,[b] Rochel M. Lago,[a] Clésia C. Nascentes[a] and Letícia M. Costa[*,a]*

[a]Departamento de Química, ICEx, Universidade Federal de Minas Gerais,
Av. Antônio Carlos, 6627, 31270-901 Belo Horizonte-MG, Brazil

[b]Centro de Desenvolvimento da Tecnologia Nuclear,
Av. Antônio Carlos, 6627, CP 941, 30161-970 Belo Horizonte-MG, Brazil

In this work, *Ricinus communis* L. press cake waste from biodiesel production was used to produce a versatile reactive material for environmental applications. The biodiesel cake waste was impregnated with Fe^{III} at different concentrations (19-45 wt.%) and treated at 400, 600 and 800 °C. Mössbauer, X-ray diffraction (XRD), thermogravimetric analysis (TG/DTA), scanning electron microscope (SEM), elemental analysis CHN, Raman, potentiometric titration, saturation magnetization and Brunauer-Emmett-Teller (BET) analyses showed that the materials prepared at 400 °C are composed mainly of a graphitic and amorphous carbon containing dispersed magnetite (Fe$_3$O$_4$). At higher temperatures, metallic iron (Fe^0) and iron carbide (Fe$_3$C) are the predominant phases well dispersed in the carbon porous structure. These reduced iron species, Fe$_3$O$_4$ and Fe^0, are active for the reduction of different hazardous contaminants. Preliminary experiments showed very high activities for the reduction and removal of aqueous Cr^{VI}.

Keywords: biodiesel press cake, reactive Fe phases, carbon support, hexavalent chromium

Introduction

Biodiesel press cakes are solid materials obtained after mechanical pressing and oil extraction consisting mainly of lignocellulosic fibers. These biodiesel wastes have been used mainly for energy production which is not economically interesting due to the low calorific content.[1] Some cakes have also been used for animal feeding.[2] However, due to the deficiency of proteins and the presence of some toxic compounds some biodiesel cakes cannot be used for nutrition purposes. For example, castor bean (*Ricinus communis* L.) has high oil contents and it has been intensively investigated for biodiesel production. However, due to the presence of ricine, the produced cake is highly toxic and cannot be used in feed blends for animals.[3] Therefore, processes to convert biodiesel cake wastes into new materials for relevant applications are of considerable interest.

In this work, it was studied the use of biodiesel cake waste to produce a versatile reactive and adsorbent composite based on reduced Fe surface species and porous carbon for different environmental applications. This composite was produced by a simple process consisting of Fe^{III} impregnation on the lignocellulosic cake waste followed by thermal treatment under controlled conditions to form a multifunctional material. The Fe^{III} is reduced to form Fe^{II} and Fe^0 species whereas the lignocellulosic precursor is decomposed to form a porous carbon with oxygen surface groups (Figure 1).

The reduction of Fe^{III} to form reactive Fe species has been previously reported in different systems, such as tar
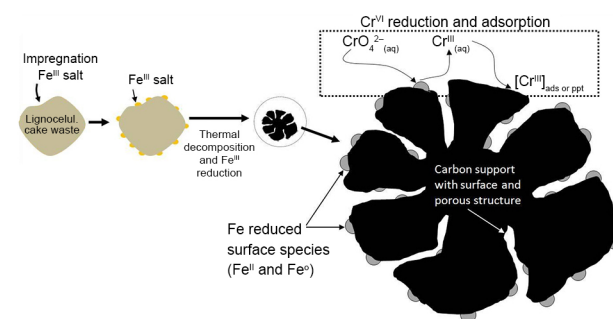
Figure 1. Schematic representation of the preparation of the reactive material for Cr^{VI} reduction.

*e-mail: leticia@qui.ufmg.br

pitch,[4,5] activated carbon[6] and H_2.[7-9] These surface Fe species can be used for the reduction of different environmental contaminants such as nitrate,[10-12] organochlorine pesticides,[13] as permeable reactive barriers[5,14] and for oxidations via the Fenton reaction.[8,15,16] Iron species can also reduce the hazardous Cr^{VI} which is widely used in industries such as leather tanning, electroplating, pigment production, wood treatment and others.[17]

Hereon, preliminary results on the preparation of these reactive composites and their use for the reduction and removal of the hazardous Cr^{VI} will be presented.

Experimental

Production of the reactive composites

Ricinus communis L. press cake used as carbon precursor was dried for 72 h at 60 °C. The impregnation of iron was carried out in 50 g of biomass using 68.5, 126 and 162 g of $Fe(NO_3)_3.9H_2O$ solubilized in approximately 300 mL of ethyl alcohol to produce composites Fe/C with 19, 35 and 45 wt.% of Fe. The biomass suspension was dried under stirring and treated at 400, 600 and 800 °C for 1 h in a horizontal tubular furnace using a heating rate of 10 °C min^{-1} under N_2 at a flow rate of 100 cm^3 min^{-1}.

Characterization of composites

The pore structure of composites was analyzed by nitrogen sorption at 77 K using an automatic Autosorb apparatus (Quantachrome Corporation). Fourier transform infrared spectroscopy (FTIR) analyses were carried out in Perkin Elmer BX.

The number of oxygen sites in the surface was analyzed by a potentiometric titration (0.050 g of composites in 25.0 mL of 0.5 mol L^{-1} $NaNO_3$) at 25 ± 1 °C using an automatic Titroprocessor (Methrom, mod. 670). The experimental data were adjusted using a non-linear regression program, as described in previous studies.[18] The zero charge point (pH_{zpc}) was determined using the solid addition method. In this method, 25 mL of aqueous solutions at different pH values (1-11) were mixed with 0.0125 g of sample. The suspensions were sealed and stirred at room temperature for 24 h at 180 rpm. Subsequently, the pH of the supernatant was measured and the difference between the initial pH (pH_i) and final pH (pH_f) values was plotted as a function of pH_i.

The microstructure of the magnetic composites was investigated by scanning electron microscopy (SEM) with JOEL, model JSM-6360LV. The crystal structure was characterized by a Rigaku diffractometer with Cu Kα

radiation. Thermogravimetric analyses (TGA) were carried out with a Shimadzu TGA60H thermo balance device with air flow (100 mL min^{-1}), at 10 °C min^{-1}. Elemental analysis was conducted on CHN/S 2400 series II (PerkinElmer). Raman spectra were obtained in a Bruker Senterra spectrometer, with excitation wavelength of 632.8 nm and a helium-neon laser. The laser targeted the sample through an Olympus BX-51 microscope (20× magnification). Mössbauer spectra were obtained at room temperature employing a conventional spectrophotometer with constant acceleration, [57]Co source in Rh matrix, using α-Fe as reference. Measurements were made of samples pulverized without application of external magnetic field. The spectra were fitted using a numerical program (NORMOS). Magnetization measurements were obtained using a LakeShore 7404 vibrating sample magnetometer with noise base of 1×10^{-6} emu, time constant of 100 ms and averaging time of 2 s *per* point, and measurement time of 101 s. Fields were swept at 1400 Oe s^{-1}. All measurements were performed at room temperature.

Batch adsorption studies

Preparation of Cr^{VI} solution

A hexavalent chromium solution was prepared by dissolving 2.3 g $K_2Cr_2O_7$ in 1000 mL of deionized water. The initial pH was adjusted to 4 with 1 mol L^{-1} HCl or NaOH and experimental solutions were obtained by successive dilutions.

Cr^{VI} removal

The Cr^{VI} removal experiments were carried out using 10 mg of the reactive composite in 10 mL of 50 mg L^{-1} Cr^{VI} solution at 25 °C for 4 h at pH 4 which guarantees reaction and adsorption equilibrium. After reaction, the composites were separated from solution by a magnet and the total chromium concentration was measured by flame atomic absorption spectrometry (FAAS).

Results and Discussion

The composites prepared with different iron contents and temperatures have been named hereon as CXFeY, where X is the iron content (0, 19, 35 or 45 wt.%) and Y is the treatment temperature (400, 600 or 800 °C). X-ray diffraction (XRD) powder diffractions analyses for the composites showed in general low crystallinity (see Supplementary Information for all XRD patterns, Figure S1). The XRD of the composites containing 45% Fe reduced at 400, 600 and 800 °C suggested the presence of the iron reduced phases Fe_3O_4, Fe^0 and Fe_3C (Figure 2).

Mössbauer analyses of the composites containing 45 wt.% Fe treated at 400, 600 and 800 °C are shown in Figure 3.
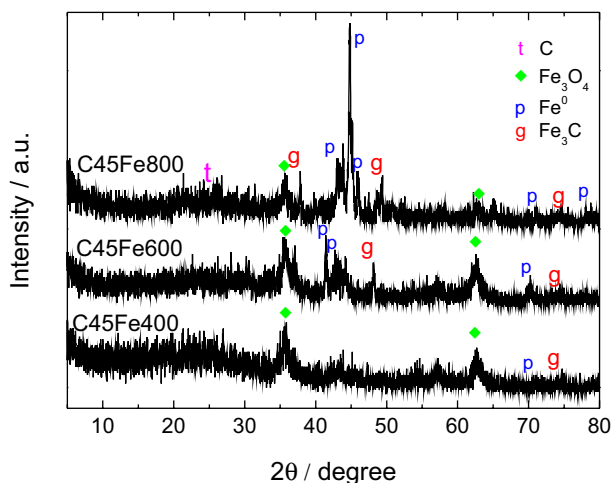
Figure 2. Powder XRD patterns for the composites with 45 wt.% Fe treated at different temperatures.
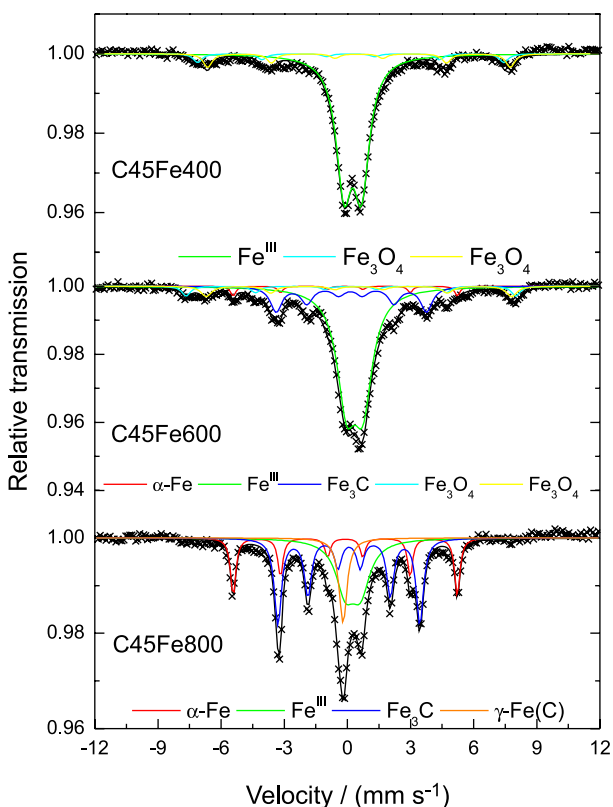
Figure 3. Mössbauer spectra at 298 K for the samples C45Fe400, C45Fe600 and C45Fe800.

The Mössbauer data for the sample C45Fe400 confirms the presence of magnetite Fe_3O_4 (with 17% relative area) and dispersed Fe^{III} (83%). After treatment at 600 °C (C45Fe600), the main reduced phases observed were α-Fe (3% relative area), γ-Fe (7%), Fe_3C (19%), Fe_3O_4 (6%) and disperse Fe^{III}

(65%). At 800 °C (C45Fe800) a significant Fe^{III} reduction was observed with concentration decrease to 29%, whereas reduced iron phases increased, i.e., α-Fe (20%), γ-Fe (11%) and Fe_3C (40%). The Fe^{III} present in small amounts was likely formed by the oxidation of reduced iron species when the sample was exposed to air at room temperature. A general idea of the Fe phases present in the different composites is shown in Figure 4. The Mössbauer spectra and hyperfine parameters for all the composites are shown in Supplementary Information (Figure S2 and Table S1).
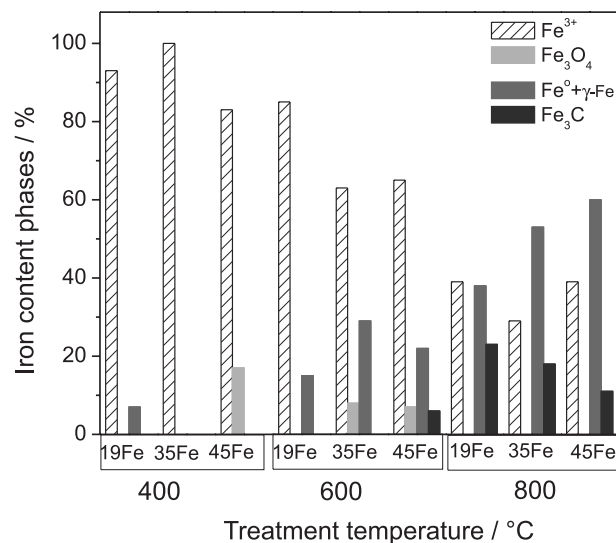
Figure 4. Iron content phases for the composites containing 19, 35 and 45 wt.% Fe treated at 400, 600 and 800 °C.

Similar results were found by Oliveira *et al.*[19] and Mendonça *et al.*[20] where Fe^{II} and Fe^{III} predominate at low temperatures and Fe^0 and Fe_3C are formed above 550 °C. These results suggest that Fe^{III} can be reduced by carbon according to the simplified equations 1, 2 and 3.

$$Fe^{III}/presscake \xrightarrow{N_2 / 400 °C} Fe_3O_4 + C + CO_x/H_2O/volatiles \quad (1)$$

$$Fe_3O_4 + C \xrightarrow{N_2 / 600 °C} Fe^0 + 2 CO_x \quad (2)$$

$$Fe^0 + C \xrightarrow{N_2 / 800 °C} Fe_3C \quad (3)$$
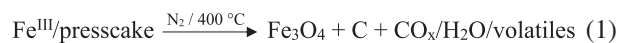
Magnetization values varying from 0.1 to 20.1 emu g^{-1} (see Supplementary Information, Table S2) were found for the obtained composites, which are due to the formation of the magnetic phases Fe_3O_4, Fe^0 and Fe_3C showed by Mössbauer.

Raman spectra (Supplementary Information, Figures S3 and S4) for all obtained composites showed the two typical bands for carbon materials, i.e., the G-band related to tangential vibration modes of well-organized graphitic structures at 1500 cm^{-1}, and the D-band at 1300 cm^{-1}

Table 1. BET surface areas and pore size distribution of composites treated at 400, 600 and 800 °C

Sample	Treatment temperature / °C					
	400		600		800	
	$S_{BET}{}^a$ / (m² g⁻¹)	D^b / nm	$S_{BET}{}^a$ / (m²g⁻¹)	D^b / nm	$S_{BET}{}^a$ / (m² g⁻¹)	D^b / nm
C0Fe	2	–	0	–	0	–
C19Fe	0	–	44	3	40	3
C35Fe	4	–	60	3	79	4
C45Fe	0	–	26	3	67	4

^{a}Surface area (S_{BET}); ^{b}distribution (D) average pore size.

assigned to defective carbon structures, such as amorphous carbon.[21] The G' band near 2700 cm⁻¹ confirms the presence of graphite like structures.[21]

The carbon contents in the pyrolized materials were determined by CHN analyses. TGA (Supplementary Information, Figure S5) showed a complex behavior due to at least three reactions taking place simultaneously: the oxidation of carbon, the oxidation of Fe phases and the reaction of Fe oxide phases with the carbon. The exothermic weight losses near 350 °C related to the oxidation of the carbon support were used to confirm the percentage of C.[22] The carbon contents determined by CHN analyses for the composites obtained after treatment at 800 °C were 58, 50 and 45% for the composites C19Fe, C35Fe and C45Fe, respectively (see all analyses in Supplementary Information, Table S3).

The composites were also analyzed by N₂ adsorption to determine the surface area (S_{BET}) and pore distribution (D). The obtained results are shown in Table 1.

The composites obtained at 400 °C did not show any significant surface area. On the other hand, composites with surface area up to 79 m² g⁻¹ with the presence of porous with average diameter of ca. 3-4 nm, were obtained at 600 and 800 °C. These results clearly show that the presence of Fe[III] has an activation effect to generate surface area and a mesoporosity.

The morphology of the composites was investigated by SEM and the images obtained presented in Figure 5.

The SEM images suggest that the thermal treatment of the cake produces irregular particles with sizes varying from few micrometers up to 500 μm with the presence of internal large pore spaces. SEM images show that upon impregnation of Fe nitrate and thermal treatment a bright surface layer is formed, which is related to Fe species as suggested by energy dispersive spectroscopy (EDS) analyses.

Potentiometric titration experiments showed the presence of surface groups, likely related to oxygen functionalities. Estimation of pKa of these groups suggests the presence of carboxylic groups (pKa < 6), lactone and quinine groups with pKa > 7 (see Supplementary Information, Table S4). It is interesting to observe that the obtained zero charge point (ZPC) for the composites ranged from 8 at 10 which cannot be explained by these oxygen surface groups with typical ZPC 2-4.[23] These results suggest that the iron oxides (with pH_{ZPC} typically above 8)[24] present on the carbon surface are likely responsible for the observed surface charges.

Batch experiments of Cr[VI] removal from aqueous solutions were carried out using the 12 different prepared composites (Figure 6).

The lignocellulosic precursor before carbonization did not show any activity for Cr[VI] reduction nor adsorption. The cake (without Fe) treated at 400-800 °C showed ca. 36-37% Cr[VI] removal likely due to the reduction of Cr[VI] (CrO_4^{2-} and $Cr_2O_7^{2-}$) by the carbon surface and some adsorption. Similar results were obtained for the composites Fe/C treated at 400 °C. This result suggests that the Fe species present in the composites obtained at 400 °C have no effect on the Cr[VI] reduction. On the other hand, treatment at 600 and 800 °C showed a significant increase in the Cr[VI] reduction efficiency. In fact, 80% Cr[VI] reduction was monitored by the diphenylcarbazide method[25] for the composite C35Fe800 (Supplementary Information, Figure S6). It is interesting to observe that the C0Fe800 (without Fe) showed only 50% Cr[VI] reduction. This result confirms the strong activity of Fe for the reduction of Cr[VI] (Supplementary Information, Figure S7).

The highest Cr[VI] removal was obtained for the composite C45Fe800 with 85% removal. This increase in Cr[VI] removal efficiency is related to the presence of reduced Fe phases in the composite. At lower Cr[VI] concentration (10 mg L⁻¹) the removal efficiency was 95% reaching a final chromium concentration of 0.5 mg L⁻¹.

The Cr[VI] removal capacity was investigated in detail for the composite C45Fe800 varying the Cr[VI] solution from 70 up to 700 mg L⁻¹. Figure 7 shows the equilibrium concentration and the respective removal capacity in terms of mg_{Cr} g⁻¹.
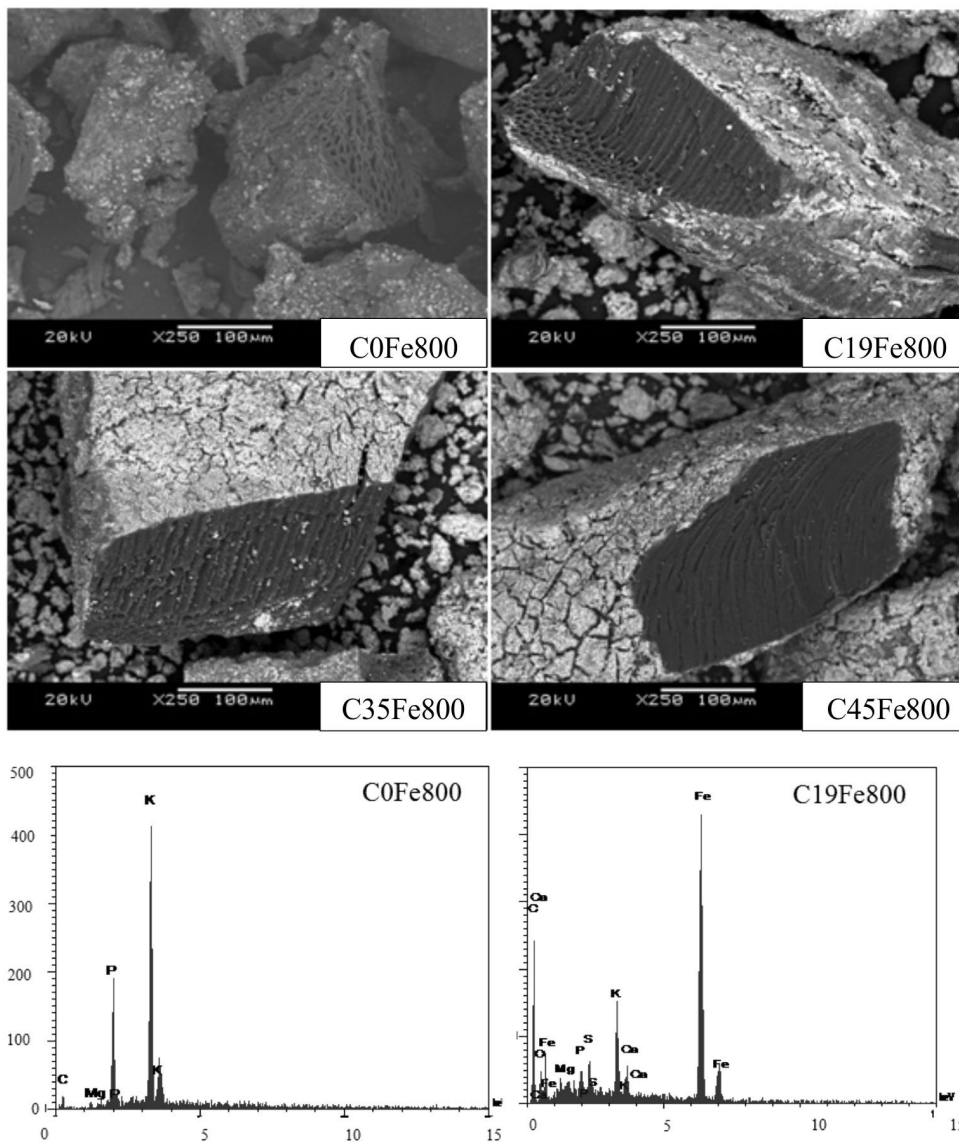
Figure 5. SEM-EDS micrographs of composites produced at 800 °C.
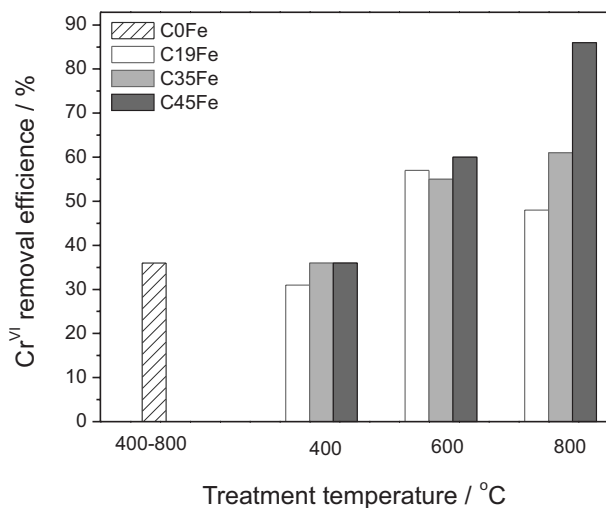
Figure 6. Cr^{VI} removal efficiency using the pure carbon (no Fe) and the composites treated at different temperatures at pH 4.
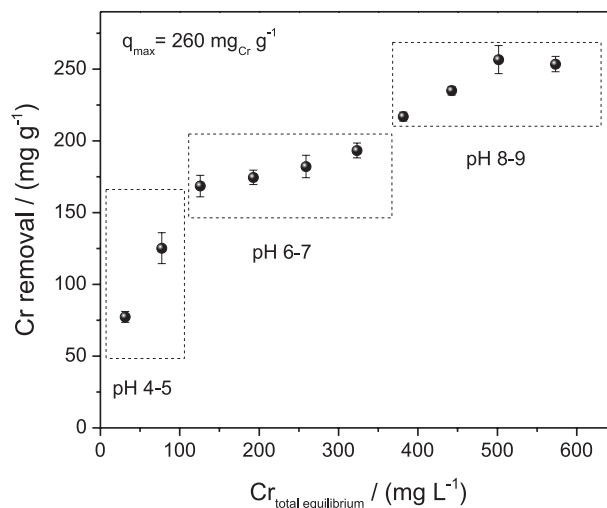
Figure 7. Cr^{VI} removal in the presence of the C45Fe800 composite at 25 °C.

It is interesting to observe that the removal efficiency increases as the Cr concentration increases until a *plateou* is produced between Cr total equilibrium concentrations of 200-300 mg L^{-1}. At higher $Cr_2O_7^{2-}$ concentrations the Cr removal increases again until the maximum value of 260 mg$_{Cr}$ g^{-1}. This value is higher compared to several Cr^{VI} removal capacities reported in the literature for different carbon based materials, e.g., carbon nanosphere/Fe_2O_3 (200 mg$_{Cr}$ g^{-1}),[25] modified graphene oxide (120 mg$_{Cr}$ g^{-1}),[26] MWNT/Fe_2O_3 (90 mg$_{Cr}$ g^{-1}),[27] activated carbon by biomass/Fe^0 (12 mg$_{Cr}$ g^{-1}),[28] and carbon-encapsulated/Fe^0 (10 mg$_{Cr}$ g^{-1}).[29]

The composites also showed much higher removal efficiency (260 mg$_{Cr}$ g^{-1}) compared to 0.45 mg$_{Cr}$ g^{-1} obtained for other low cost lignocellulosic materials, e.g., olive mill waste.[30]

Measurements of the pH after the equilibrium showed three main groups of final pH: for low initial Cr concentrations the final pH was 4-5, increasing to 6-7 and finally 8-9 for the higher $Cr_2O_7^{2-}$ concentrations. This increase in the pH is related to the $Cr_2O_7^{2-}$ reduction which consumes H$^+$ as represented by the simple equation 4.

$$Cr_2O_7^{2-} + 2\,Fe^0 + 14\,H^+ \rightleftharpoons 2\,Cr^{III} + 2\,Fe^{III} + 7\,H_2O \quad (4)$$
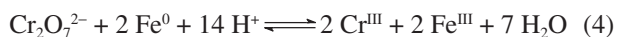
Based on these considerations, one can envisage some possible Cr removal mechanisms as a function of the pH. Initially, at low Cr concentration and pH 4-5, Cr^{VI} (in the form of the anions $Cr_2O_7^{2-}$ or CrO_4^{2-}) can be adsorbed due to the positive surface charges on the composite (pH$_{ZPC}$ 10). Also, in these conditions Cr^{VI} can be reduced to Cr^{III}. However, this Cr^{III} is not adsorbed on the composite and probably remains in solution due to the low pH. In these conditions pH 4, [OH$^-$] = 10^{-10} mol L^{-1} and Kps for Cr(OH)$_3$ (6 × 10^{-31}),[31] Cr^{III} should have a significant solubility in water. Therefore, Cr^{III} remains in solution and does not decrease the Cr removal (Figure 8).
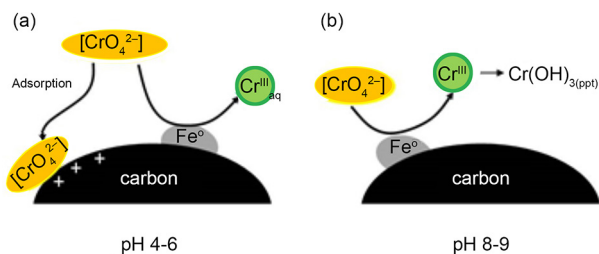
Figure 8. Schematic representation of Cr reduction, (a) adsorption; (b) precipitation in different pH.

As the experiments were carried out with higher Cr^{VI} initial concentrations, the final pH increased reaching values near 9. Under these conditions, the surface tends

to zero charge. The reduction Cr^{VI} takes place and the Cr^{III} formed can precipitate as Cr(OH)$_3$ due to the high pH or adsorbed onto oxygen surface groups by an ion exchange mechanism (Figure 8).

Conclusions

Ricinus communis L. biodiesel press cake waste can be used as a good precursor to produce a versatile reactive composite for environmental applications by a simple process consisting of Fe^{III} impregnation followed by thermal treatment under controlled conditions. These multifunctional materials showed interesting properties for environmental applications, e.g., well dispersed excellent reactive phases (Fe$_3$O$_4$ and Fe^0) to reduce different hazardous contaminants and porous carbon support with surface oxygen groups with special adsorption properties. Moreover, the use of a lignocellulosic waste, e.g., cake, the relatively low cost of energy for thermal treatment (R\$ 0.01-0.03 kg^{-1})[32,33] and the possibility to use iron rich wastes suggest an interesting economical feasibility for this material. Preliminary experiments showed very high activities for the reduction and removal of aqueous Cr^{VI}.

Supplementary Information

Supplementary information is available free of charge at http://jbcs.sbq.org.br as PDF file.

Acknowledgements

References

1. Kumar, N.; Varun; Chauhan, S. R.; *Renewable Sustainable Energy Rev.* **2013**, *21*, 633.

2. Martín, C.; Moure, A.; Martín, G.; Carrilho, E.; Domíngyes, H.; Parajó, J. C.; *Biomass Bioenergy* **2010**, *34*, 533.

3. Andrade, F. P.; Nascentes, C. C.; Costa, L. M.; *Anal. Lett.* **2012**, *45*, 2833.

4. Amorim, C. C.; Leão, M. M. D.; Dutra, P. R.; Tristão, J. C.; Magalhães, F.; Lago, R. M.; *Chemosphere* **2014**, *109*, 143.

5. Magalhães, F.; Pereira, M. B. C.; Fabris, J. D.; Bottrel, S. A.; Sansiviero, M. T.; Amaya, A.; Tancredi, M.; Lago, R. M.; *J. Hazard. Mater.* **2009**, *165*, 1016.

6. Pereira, M. C.; Coelho, F. S.; Nascentes, C. C.; Fabris, J. D.; Araújo, M. H.; Sapag, K.; Oliveira, L. C. A.; Lago, R. M.; *Chemosphere* **2010**, *81*, 7.

7. Amorim, C. C.; Dutra, P. R.; Leão, M. M. D.; Pereira, M. C.; Henriques, A. B.; Fabris, J. D.; Lago, R. M.; *Chem. Eng. J.* **2012**, *209*, 645.

8. Oliveira, P. E. F.; Oliveira, L. D.; Ardisson, J. D.; Lago, R. M.; *J. Hazard. Mater.* **2011**, *194*, 393.

9. Coelho, F. S.; Ardisson, J. D.; Moura, F. C. C.; Lago, R. M.; Murad, E.; Fabris, J. D.; *Chemosphere* **2008**, *71*, 90.

10. Mossa-Hossein, S.; Ataie-Ashtiani, B.; Kholghi, M.; *Desalination* **2011**, *276*, 214.

11. Hori, M.; Shozugawa, K.; Matsuo, M.; *Sci. Total Environ.* **2010**, *408*, 3418.

12. Villacís-García, M.; Villalobos, M.; Gutiérrez-Ruiz, M.; *J. Hazard. Mater.* **2015**, *281*, 77.

13. Cong, X.; Xue, N.; Wang, S.; Li, K.; Li, F.; *Sci. Total Environ.* **2010**, *408*, 3418.

14. Ruhl, A. S.; Jekel, M.; *Chem. Eng. J.* **2012**, *213*, 245.

15. Soares, P. A.; Batalha, M.; Souza, S. M. A. G. U.; Boaventura, R. A. R.; Vilar, V. J. P.; *J. Environ. Manage.* **2015**, *152*, 120.

16. Li, H.; Li, Y.; Xiang, L.; Huang, Q.; Zhang, H.; Sivaiah, M. V.; Baron, F.; Barrault, J.; Petit, S.; Valange, S.; Qiu, J.; *J. Hazard. Mater.* **2015**, *287*, 32.

17. Mohan, D.; Junior, C. U. P.; *J. Hazard. Mater.* **2006**, *B137*, 762.

18. Gorgulho, H. F.; Mesquita, J. P.; Gonçalves, F.; Pereira, M. F. R.; Figueiredo, J. L.; *Carbon* **2008**, *46*, 1544.

19. Oliveira, L. C. A.; Petkowicz, D. I.; Smaniotto, A.; Pergher, S. B. C.; *Water Res.* **2004**, *38*, 3699.

20. Mendonça, F. G.; Ardisson, J. D.; Rosmaninho, M. G.; Lago, R. M.; Tristão, J. C.; *Hyperfine Interact.* **2011**, *202*, 123.

21. Salame, I. I.; Bandosz, T. J.; *J. Colloid Interface Sci.* **2001**, *240*, 252.

22. Shimada, T.; Sugai, T.; Fantini, C.; Souza, M.; Cançado, L. G.; Jorio, A.; Pimenta, M. A.; Saito, R.; Gruneis, A.; Dresselhaus, G. M. S.; Ohno, Y.; Mizutani, T.; Shinohara, H.; *Carbon* **2005**, *43*, 1049.

23. Mahmudov, R.; Huang, C. P.; *Sep. Purif. Technol.* **2010**, *70*, 329.

24. Hlavay, J.; Polyák, K.; *J. Colloid Interface Sci.* **2005**, *284*, 71.

25. Zhang, L.; Sun, Q.; Liu, D.; Lu, A.; *J. Mater. Chem. A* **2013**, *1*, 9477.

26. Fan, L. L.; Luo, C. N.; Sun, M.; Qiu, H. M.; *J. Mater. Chem.* **2012**, *22*, 24577.

27. Gupta, V. K.; Agarwal, S.; Saleh, T. A.; *Water Res.* **2011**, *45*, 2207.

28. Liu, W.; Zhang, J.; Zhang, C.; Wang, Y.; Li, Y.; *Chem. Eng. J.* **2010**, *162*, 677.

29. Zhuang, L.; Li, Q.; Chen, J.; Ma, B.; Chen, S.; *Chem. Eng. J.* **2014**, *253*, 24.

30. Mosca, M.; Cuomo, F.; Lopez, F.; Palumbo, G.; Bufalo, G.; Ambrosone, L.; *Desalin. Water Treat.* **2015**, *54*, 275.

31. Skoog, D. A.; West, D. M.; Holler, T. A.; Crouch, S. R.; *Fundamentos de Química Analítica*, 8th ed.; Bookman: Porto Alegre, 2002.

32. Karayildirim, T.; Yanik, J.; Yuksel, M.; Bockhorn, H.; *Fuel* **2006**, *85*, 1498.

33. Shen, L.; Zhang, D.; *Fuel* **2003**, *82*, 465.